Spectrochimica Acta Part A: Molecular and Biomolecular Spectroscopy 292 (2023) 122400

Contents lists available at ScienceDirect

Spectrochimica Acta Part A:
Molecular and Biomolecular Spectroscopy

journal homepage: www.journals.elsevier.com/spectrochimica-acta-part-a-molecular-and-biomolecular-spectroscopy

Unveiling the tartrazine binding mode with ds–DNA by UV–visible spectroscopy, electrochemical, and QM/MM methods

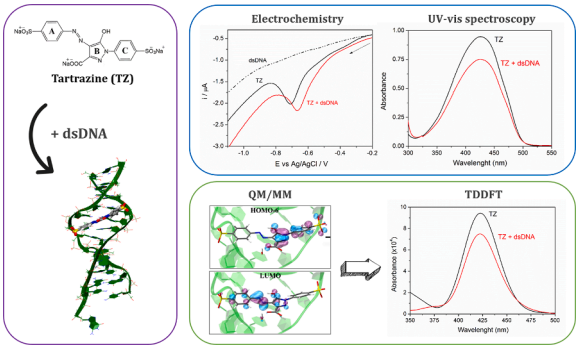
S. Arsenault-Escobar [a], J.F. Fuentes-Galvez [a], C. Orellana [b], S. Bollo [c,d], P. Sierra–Rosales [a,*], S. Miranda-Rojas [e,*]

[a] Programa Institucional de Fomento a la Investigación, Desarrollo e Innovación, Universidad Tecnológica Metropolitana, Ignacio Valdivieso 2409, P.O Box 8940577, San Joaquín, Santiago, Chile
[b] Departamento de Química, Facultad de Ciencias, Universidad de Chile, P.O. Box 653, Las Palmeras 3425, Ñuñoa, Santiago, Chile
[c] Centro de Investigación de Procesos Redox (CiPRex), Universidad de Chile. Sergio Livingstone Polhammer 1007, Independencia, Santiago, Chile
[d] Advanced Center for Chronic Diseases (ACCDiS), Universidad de Chile. Sergio Livingstone Polhammer 1007, Independencia, Santiago, Chile
[e] Departamento de Ciencias Químicas, Facultad de Ciencias Exactas, Universidad Andres Bello, República 275, Santiago, Chile

HIGHLIGHTS

- We proved that tartrazine interacts with dsDNA via minor-groove binding mode.
- The experimental binding constants of tartrazine-dsDNA are similar between methods.
- Computational models revealed the preference of tartrazine for adenine and thymine.

GRAPHICAL ABSTRACT



ARTICLE INFO

Keywords:
Tartrazine
Groove binding
DNA interaction
QM/MM
Binding constant

ABSTRACT

Here, we studied the interaction between the food colorant tartrazine (TZ) and double stranded DNA (dsDNA), using spectroscopic, electrochemical, and computational methods such as QM/MM combined with TD-DFT. Despite the UV–vis spectroscopy is widely used to study the interaction between molecules, for the case of TZ there are discrepancies in the analyses presented in the literature available, presenting both hyperchromic and hypochromic effects and consequently different rationalizations for their results. Herein we propose the combination of UV–vis experiments with the design of high-level computational models capable of reproducing the experimental behavior to finally define the proper binding mode at the molecular scale together with the rationalization of the experimental optical response due to the complex formation. To complement the UV–vis experiments, we propose the use of electrochemical measurements, to support the results obtained through UV–vis spectroscopy, as it has been successfully used for the determination of interaction modes between small molecules and biomolecules in any condition. Our UV–vis spectroscopy experiments showed only a hypochromic effect of the absorption spectra of TZ after interaction with DNA, indicative of TZ being deeply buried in the DNA

* Corresponding authors.
E-mail addresses: psierra@utem.cl (P. Sierra–Rosales), sebastian.miranda@unab.cl (S. Miranda-Rojas).

https://doi.org/10.1016/j.saa.2023.122400
Received 30 September 2022; Received in revised form 31 December 2022; Accepted 19 January 2023
Available online 27 January 2023
1386-1425/© 2023 Elsevier B.V. All rights reserved.

structure. The effect of ionic strength in the experimental procedures led to the dissociation of TZ, thus indicating that the interaction mode was groove binding. On the other hand, the electrochemical studies showed an irreversible reduction peak of TZ, which after the interaction with DNA exhibited a positive shift in potential that can be attributed to groove binding. The binding constant for TZ-DNA was calculated as $4.45\,x\,10^4\,M^{-1}$ (UV–vis) and $5.75\,x\,10^4\,M^{-1}$ (electrochemistry), in line with other groove binder azo dyes. Finally, through the QM/MM calculations we found that the minor-groove binding mode interacting in zones rich in adenine and thymine was the model best suited to reproduce the experimental UV–vis response.

1. Introduction

Tartrazine (TZ) is a yellow synthetic azo dye used for coloring food, drugs, and cosmetic products. As an azo dye, its degradation/metabolism produces aromatic amines in the body, which are considered highly toxic. These molecules can damage urinary organs, the kidney, the stomach, and the liver [1,2]. For example, the food azo dye Sudan I has both genotoxic and carcinogenic effects, and international panels such as the European Food Safety Authority (EFSA) assume that other azo dyes with similar structures are potentially genotoxic and possibly carcinogenic [3]. Therefore, a series of studies on azo dye interactions with biomolecules such as human hemoglobin [1], albumins [4], lysozyme [5], and deoxyribonucleic acid (DNA) [6–9] have been reported.

Among these biomolecules, the interaction with DNA is one of the most important aspects in several areas of research because it helps to understand the mechanism of action or toxicity of different molecules. It is well known that DNA can be found unwrapped under several conditions of normal DNA reading and replication. The interaction of small molecules and DNA has been also demonstrated under physiological conditions, not only for dyes, but for a series of molecules, including drugs, which support their mechanism of action via interaction with DNA by different binding mechanisms [10,11]. The interaction between molecules and DNA has been categorized into three types: (i) electrostatic (between positively charged molecules and the negative DNA phosphate groups), (ii) groove binding, and (iii) intercalation (associated with planar aromatic molecules) [11–13]. These types of interactions can change the DNA conformation, interrupt protein-DNA interactions and potentially lead to the breakage of DNA strands. All of these events can have substantial effects on gene expression [10,12].

The commonly used techniques for studying the interaction between small molecules and DNA are UV–visible spectroscopy, fluorescence spectroscopy, circular dichroism spectroscopy, viscosity measurement studies, isothermal titration calorimetry, Fourier transform infrared spectroscopy, and voltammetry measurements [12]. In this respect, voltammetric techniques can work as an excellent complement to other techniques based on the optical response of the complex, especially when the results show weak absorption or fluorescence spectra and/or overlapping of electronic transitions with DNA. UV–visible spectroscopy is one of the most used techniques because of its simplicity. The interaction between small molecules and DNA leads to changes in the UV–visible spectra of both molecules. In this context, to be able to correlate the band intensity (hyper- or hypochromic effect) and/or any shift in the position of the peak in the spectra (batho- or hypsochromic shift) to a specific interaction mode is an important target of research, as it provides the insights to predict the interaction mode of chemically similar molecules depending on their optical response. According to Rehman et al. [14], when small molecules intercalate into DNA, the UV–visible spectrum of the molecule shows a bathochromic shift as well as a hypochromic effect. In the case of groove binding interactions, a smaller or no bathochromic shift is observed. On the other hand, in the case of electrostatic interactions, Horakova et al. [15] indicated that a hyperchromic effect is detected. If the band observed for the interaction comes from DNA absorption, the hyperchromism could be associated with partial uncoiling of the double helix, which exposes more bases of the DNA to the solution, explaining the increase in the DNA absorption band [16]. Therefore, the hyper- or hypochromic effect must be analyzed and assigned carefully, as there are several variables involved in the observed spectral changes after complexation with DNA.

For food colorants, a few studies have confirmed the interaction of DNA with TZ [6,9,17], sunset yellow (SY) [7,16], carmoisine (CR) [18,19] and Allura Red (AR) [20] by UV–visible absorption spectroscopy. These four colorants have two aromatic moieties connected by an azo group; therefore, a similar interaction mode between them and DNA was expected. For SY, Asaadi et al. [7] added DNA to different concentrations of SY observing a hypochromic effect on the main band of the colorant, from which calculated an intrinsic binding constant (K) of 2.1×10^3 M^{-1}. Also, based on other experiments, they stated that the interaction of SY with DNA is a combination of intercalation and electrostatic modes due to the planar structure and positive charges of the colorant. Nevertheless, the problem with that binding mode proposal is that SY is in fact not planar; therefore, the intercalation mode should not be favored. In addition, the pK_a of the colorant is 10.5 [21], which means that below pH 8.0, the molecule is actually in an anionic state, having a repulsive effect toward electrostatic interactions. On the other hand, Kashanian et al. [16] observed a hyperchromic effect for the same experiment and attributed the changes in the spectra to an external contact of the colorant with DNA, with a K of 7.0×10^4 M^{-1}. The authors concluded that the interaction mode of SY is groove binding by comparison of the K value with those of other groove binder agents reported. For CR, two reports showed opposite effects in the UV–vis spectra when different amounts of DNA were added to a fixed concentration of CR. Arvin et al. [19] observed a hyperchromism tendency with a K of 6.2×10^4 M^{-1}. The interaction of CR with DNA was explained by the formation of hydrogen bonds between the amino and hydroxyl groups of the colorant with the DNA bases. On the other hand, Basu et al. [18] observed a hypochromic effect upon the addition of increasing amounts of DNA, indicating that the spectral changes can be attributed to a strong interaction between the ligand and the DNA base pair. The K value obtained was 2.9×10^4 M^{-1}, and the groove binding mode was proposed using other techniques instead of spectral analysis. In the case of the red colorant AR, a hypochromism effect was observed after the addition of increasing amounts of DNA with a K of 7.5×10^5 M^{-1}. The groove binding mode was deduced by comparison of the K value with those of other well-established groove binders [20]. Finally, for the case of TZ, the UV–vis spectra found in the literature also presented inconclusive and opposite results. Kashanian et al. [17] studied the interaction of TZ with DNA at a neutral pH of 7.4, and their results showed a hyperchromic effect in the UV absorption band of TZ. According to the authors, the binding of TZ damages the DNA structure and interacts with a K value of 3.75×10^4 M^{-1}. Using other techniques, the authors indicated that the interaction mode is groove binding. On the other side, Basu et al. [6], after conducting the same experiment, observed a hypochromic change after the complexation of TZ with DNA. In this case, the K value obtained for TZ was 3.53×10^4 M^{-1}, and the interaction mode through groove binding was also suggested by the results obtained with other techniques. For azo colorants, different authors proposed the same binding mode with similar values of the binding constant, but they observed opposite changes in the UV spectra. Considering that the main goal from the use of spectroscopic techniques in this context is to be able to correlate changes in the spectrum with a specific binding mode, the discrepancy between the binding mode and the optical response becomes relevant to be solved. This would provide a predictive character

to the method allowing to search similar modifications in the patterns of the UV–vis spectrum after the binding of other chemically similar small molecules to DNA.

Because of this, the combination of electrochemical methods, UV–vis spectroscopy and computational models will provide sound evidence to solve the discrepancy in the correlation between the binding mode between TZ and ds-DNA with the UV–vis response. In recent decades, the use of electrochemical techniques have also demonstrated to provide detailed insights regarding DNA-drug interactions shown by previous studies [22,23], which could be an excellent complement to the UV–visible methods due to their accessibility and low cost. The rationale behind the use of this technique comes from the fact that the peak potential and peak current of the compound change in the presence of DNA if the compound interacts with it and vice versa. Furthermore, the changes in the peak current of the molecule by the addition of increasing DNA concentration can be used for the determination of binding constants, while the shift in potential can be used to determine the mode of interaction [12]. For this purpose, some authors have reported that if the peak potential (E_p) of the molecule shifts to more negative values when it interacts with DNA, the interaction mode is dominated by electrostatic interactions. In contrast, when E_p shifts to more positive values, the interaction mode is intercalation or groove binding [22,24]. To corroborate this, authors such as Catalán et al. [22] studied the effect of the ionic strength (IS) of the medium. At low IS values, the electrostatic interaction mode between a molecule and DNA is predominant; meanwhile, at high IS values, the charges of the DNA and the molecule are shielded, which reduces noncovalent interactions mediated by electrostatic interactions [14,25].

Herein, to solve the presented discrepancy, we show the combination of UV–vis spectroscopy, electrochemical methods, and computational models including TDDFT calculations as a robust strategy to provide the necessary evidence to solve the discrepancy in the correlation between the binding mode between TZ and ds-DNA with the UV–vis response. The use of molecular models of the TZ-DNA complex and the calculation of the UV–vis spectra of several possible binding modes by using TDDFT allowed us to determine which interaction complex reproduces the experimental UV–vis, results supported by the electrochemical response and the binding mode predicted by this method. Additionally, to the best of our knowledge, there are no reports on electrochemical studies regarding the interaction between TZ and DNA or those complemented by computational models. Finally, the experimental results will be compared and used to determine the binding constant.

2. Materials and methods

2.1. Materials

Tartrazine (TZ, CAS 1934–21-0) and calf-thymus double stranded DNA (DNA, Cat. Number D4522) were obtained from Sigma-Aldrich. NaCl was purchased from Merck. Stock solutions of DNA (1000 mg/L) were prepared with Tris-EDTA buffer solution (20 mM Tris-HCl, 1 mM EDTA, pH = 8.0). The DNA concentration was determined spectrophotometrically using literature values for the molar absorption coefficient ($\varepsilon_{260} = 6600\ L\ mol^{-1}\ cm^{-1}$) [22]. Additionally, the UV absorbance ratio (260/280 nm) was measured to verify that the DNA was sufficiently free of proteins. A stock solution of TZ (0.5 mM) was prepared in 0.1 M phosphate buffer solution (PBS, pH 7.4). Ultrapure water from a Milli-Q system was used to prepare all the solutions. All chemicals were used as received.

2.2. Instruments

Voltammetric studies were conducted on a CHI 650E potentiostat (CH Instruments Inc., USA). A three-electrode cell was used with a glassy carbon electrode (GCE), 3.0 M Ag/AgCl, and a Pt wire as the working, reference, and auxiliary electrodes, respectively. A magnetic stirrer provided convective transport when necessary. Before each measurement, the GCE was polished with 0.3 μm and 0.05 μm alumina and then washed with abundant deionized water. All experiments were performed at room temperature and in triplicate.

Electrochemical measurements were carried out in 0.1 M PBS at pH 7.4. Cyclic voltammograms (CVs) and differential pulse voltammograms (DPVs) were performed over the potential range of −1.2 and −0.2 V, and the reduction peak of TZ was recorded. The DPV operating conditions were a potential increment of 0.004 V, pulse amplitude of 0.05 V, and pulse period of 0.2 s. Consecutive DNA concentrations in the range from 0.125 mM to 0.50 mM were added to the TZ solution. Before each electrochemical measurement, the solution was purged with nitrogen for at least 15 min.

UV–vis spectra for TZ-DNA interactions were obtained using a UV–visible spectrophotometer (Hitachi U2910; VISION 3.2 software). The solutions were scanned by using a 1 cm quartz cuvette. UV–visible measurements were conducted in 0.1 M PBS at pH 7.4. A constant concentration of 0.05 mM TZ was mixed with different concentrations of DNA from 0.025 to 0.40 mM. All the samples were incubated for 15 min at room temperature. The UV–vis spectra of TZ with and without DNA were recorded over the range from 200 to 550 nm.

2.3. Calf-thymus ds-DNA modelling

To generate a model of calf-thymus ds-DNA, we used the crystal structure deposited in the Protein Data Bank (PDB) with the entry 1BNA [26], which is a 12-mer sequence that has 33.3 % guanine residues and consequently 66 % G-C base pair composition. VMD (v1.9.1) [27] was used to protonate and solvate the ds-DNA structure in a rectangular box of TIP3P water molecules, followed by the addition of ions in the form of NaCl to reach a concentration of 0.02 mol/L to ensure charge neutrality of the system. The molecular dynamics (MD) simulations were performed using periodic boundary conditions as implemented in NAMD code version 2.9 [28], and the chosen parameters for the system were those obtained from the nucleic acid CHARMM36 force field [29]. The simulations were run using a 2 fs time step, and the Langevin piston Nosé-Hoover method was used to keep the temperature and pressure at 300 K and 1 atm, respectively. The bonds involving hydrogen atoms were restrained by using the SHAKE algorithm as implemented in NAMD. The simulation protocol involved an initial minimization carried out by 10,000 steps of the conjugate gradient keeping the DNA structure fixed and allowing the water molecules to accommodate around base pairs. Then, 20,000 steps of the conjugate gradient were carried out without restrictions, followed by 1 ns of equilibration. Finally, 20 ns of production simulation was performed.

2.4. DNA-TZ complex modelling

To define a set of complexes able to represent the most likely interaction conformations between TZ and the ds-DNA, a thorough spatial exploration of binding modes was carried out by using a docking approach. For this purpose, 10 different conformations of the ds-DNA were selected from the MD simulations by taking the last snapshot every 2 ns along the 20 ns of production simulation to capture the ds-DNA in different conformations. Then, a docking procedure dividing the ds-DNA into three zones of exploration using three grids with a spacing of 0.25 Å was defined, where the lower region corresponded to the first cytosine from chain A and the upper region was the opposite end of the ds-DNA structure.

The docking calculations were performed by using AutoDock4 software [30] using the Lamarckian genetic algorithm as a search method as implemented in the program. Each docking run was carried out by setting it to 100 runs using a maximum number of evaluations set to 25,000,000 and a maximum number of generations up to 27000. This led to 30 docking calculations, from which we selected the lowest energy solution, with a total of 30 ds-DNA-TZ complexes. Each complex was

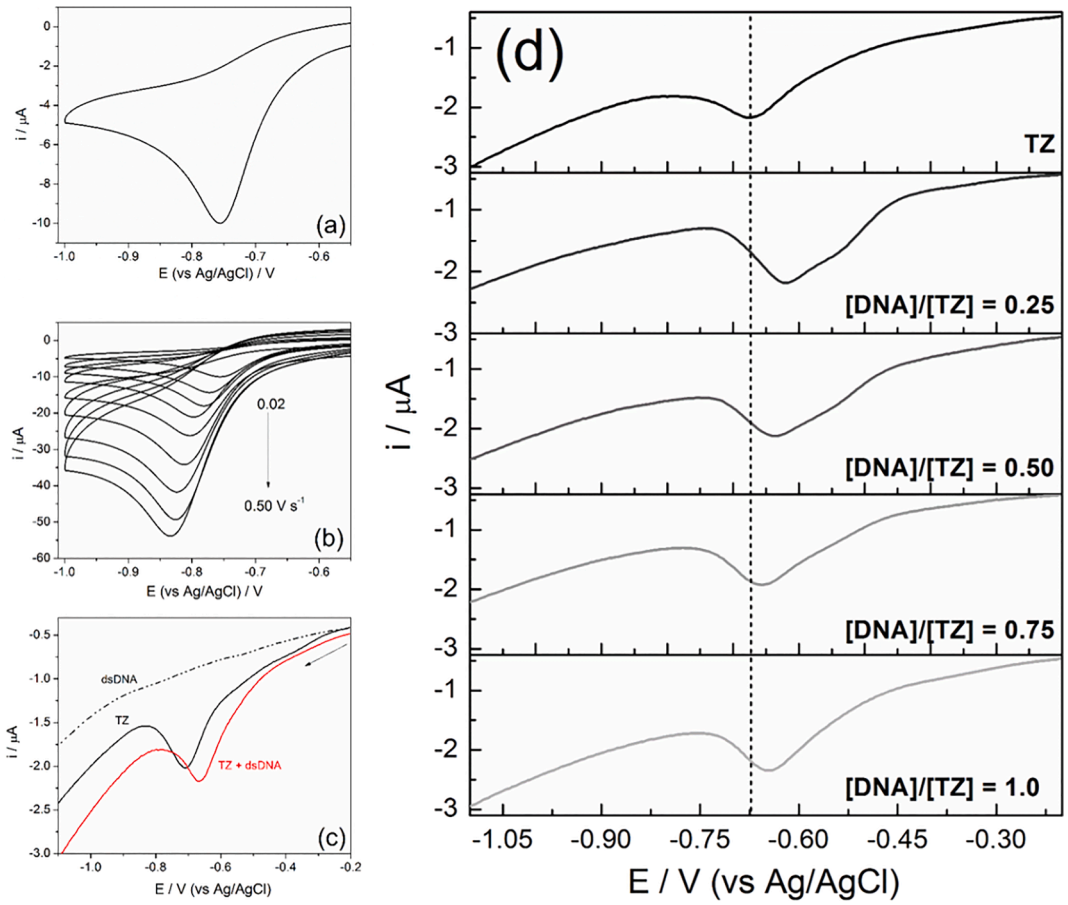


Fig. 1. (a) Cyclic voltammogram of 0.5 mM TZ. (b) Cyclic voltammograms of 0.5 mM TZ with different scan rates: 0.02, 0.04, 0.06, 0.08, 0.10, 0.20, 0.30, 0.40 and 0.50 V s^{-1}. (c) Differential pulse voltammograms of 0.5 mM TZ in the absence and presence of DNA; [DNA]/[TZ] = 3. (d) Effect of DNA concentration on the DPV of 0.5 mM TZ; [DNA]/[TZ] = 0, 0.25, 0.5, 0.75 and 1.0. Interaction time: 15 min. Supporting electrolyte: 0.1 M PBS (pH 7.4). Working electrode: glassy carbon electrode.

prepared for an MD simulation of 4 ns to evaluate the stability of the complexes in their binding conformations. Therefore, the use of the term stability throughout the study will point toward the ability to stay in the respective binding mode during the 4 ns simulation, without dissociation of TZ from the binding site. After the complex simulations, the systems that showed a stable binding mode during the simulation were selected. To obtain a representative structure of the complex from the MD simulation, we used the clustering approach implemented in VMD, which allows us to classify the visited conformations in clusters according to their RMSD and thus to define the most visited conformation. For this purpose and considering the flexibility of the ds-DNA structure, an RMSD of 2 Å was used as the cutoff. After defining the most populated cluster, the conformation with the lowest interaction energy was selected from the cluster, for which the NAMD Energy plugin implemented in VMD software was used to evaluate the noncovalent interaction energies considering only the ds-DNA and the TZ molecule without involving solving effects to obtain an estimate of the most suitable complex from the cluster. Finally, the resulting structures were set up for the QM/MM calculations.

2.5. QM/MM calculations

To obtain an accurate representation of the system under study, it is important to model the system through a full representation of the molecular complex. In addition, to provide an accurate representation of the optical response (UV–vis spectrum), a quantum chemical approach becomes mandatory. In this regard, the QM/MM approach offers an excellent balance between model size, computer time and accuracy. This approach allows us to divide the system between a quantum mechanical region (QM region) and a molecular mechanics region (MM), thus including only the most important part of the system into the QM region and the rest in the MM region to incorporate the environmental effects of the surroundings. The full QM/MM system was defined as the complete ds-DNA-TZA complex plus every water molecule at 15 Å from TZ. Meanwhile, the QM region was defined as every nucleotide base and water molecule at 3 Å from the TZA molecule. The active region, meaning the part of the QM/MM system that is allowed to move during the minimizations, was defined as TZ and every nucleic acid plus water molecules at 8 Å from the colorant. The rest of the QM/MM system was kept fixed to maintain the integrity of the model. All geometry optimizations were performed at the DFT level of theory by using the BP86 density functional [31,32]. The choice of the functional relies on its proven accuracy at reproducing both redox potential and UV–vis experimental results for azo compounds, as some of us previously reported [21]. For the basis set, the all-electron def2-SVP was used [33]. All DFT calculations include the DFT-D3 method (with the Becke-Johnson damping function) [34]. The QM/MM calculations were performed using the ChemShell suite [35] coupled with Turbomole v7.3 [36] to perform the electronic structure calculations involving the QM region. In contrast, the calculations of the MM region were performed with the DL-POLY program as implemented in the Chemshell suite. To calculate an estimate of the interaction strength between TZ and the ds-DNA system, we calculated an approximated interaction energy by using the semiempirical method implemented in xTB software [37], according to the following expression: $\Delta E_{int} = E_{complex} - (E_{ds\text{-}DNA} + E_{TZ})$. To calculate each energy, we used a full atomistic approach considering the

complete ds-DNA-TZ complexes obtained from the QM/MM calculations removing the water molecules, both treated at the semiempirical level. The energy of the ds-DNA system was calculated as the average energy from the 10 structures used for the docking procedure obtained from the 20 ns of MD, and the TZ energy was obtained from a geometry optimization of the free molecule at the same level of theory. The present approach allowed us to provide a relative scale within the set to rank the complexes according to their interaction strength.

The excitation energies for the UV–visible spectra calculations were obtained by the time-dependent perturbation theory approach (TD-DFT) [38,39] based on the random-phase approximation (RPA). Each calculation involved the estimation of 100 singlet excitation states. For each selected singlet excitation, we considered for the analysis those molecular orbital transitions with contributions larger than 20 %. For the calculations, we used as a starting point the wavefunction calculated for the QM region and included the partial charges representing the MM part of the system to model the nonlocal environment effects. All UV–vis spectra results were processed using the program SpecDis developed by Bruhn et al. [40], obtaining the fine structure UV–vis spectra and the Gaussian curve of full-width at half-maximum (FWHM) of 0.5 eV.

3. Results and discussion

3.1. Electrochemical studies

3.1.1. Electro-reduction of tartrazine

First, we characterized the electrochemical reduction of TZ at pH 7.4. The cyclic voltammetric profile of TZ is shown in Fig. 1a, where a single reduction peak was observed close to −0.750 V. The mechanism of the reduction of TZ is associated with the azo bond as follows:

$$R_1 - N = N - R_2 + 2H^+ + 2e^- \rightarrow R_1 - NH - NH - R_2 \quad (1)$$

$$R_1 - NH - NH - R_2 + 2H^+ + 2e^- \rightarrow R_1 - NH_2 + R_2 - NH_2 \quad (2)$$

The first step corresponds to the reduction of the azo colorant to obtain the hydrazine derivative via the $2H^+/2e^-$ process. Then, a second step involves the reduction of the hydrazine group, generating two aromatic amines. According to Gooding et al. [41], the reduction mechanism varies between azo compounds. In some cases, the dye shows the $4H^+/4e^-$ mechanism, mainly at low pH; meanwhile, others show a $2H^+/2e^-$ mechanism, namely, step (1), normally at high pH. This has been attributed to the fact that when the pH media is higher than 7.0, step (1) is slower, and some colorants end their reduction process in the hydrazine form. Since in our case the interaction studies were conducted at pH 7.4, it was necessary to evaluate the number of electrons to identify the mechanism involved, as it is close to the pH limit between both mechanisms. A scan rate study between 0.02 and 0.50 V s^{-1} was carried out (Fig. 1b). The current obtained was linear with the square root of the scan rate ($\nu^{1/2}$) (Fig. S1a), which is consistent with a diffusion-controlled mechanism. This was confirmed by plotting ln i versus ln ν, whose plot gives a slope of 0.50 (not shown). The reduction peak potential of TZ shifted to more negative potential values as the scan rate increased. For an irreversible system, the slope of the plot between E_p versus ln ν permits us to obtain the number of electrons involved in the redox process [21]. For TZ, the linear relationship is expressed by $E_p = -0.850 - 0.023\ln\nu$, with a slope of 23 mV (Fig. S1b), which corresponds to n = 2. Thus, the reduction of TZ involves a $2H^+/2e^-$ mechanism, indicating that TZ reduction at pH 7.4 did not form aromatic amines.

3.1.2. Tartrazine interaction with DNA in solution

The interaction studies of TZ with DNA were conducted in 0.1 M PBS at pH 7.4 by differential pulse voltammetry (DPV) at a glassy carbon electrode. The DPV technique is recommended for this study because the peak resolution is better than that of CV. The voltammetric profiles of TZ at 0.5 mM in the absence and presence of DNA are shown in Fig. 1c. DNA does not show any reduction peak in the potential range used. In the absence of DNA, the reduction of TZ occurs at −0.710 V, which positively shifted to –0.650 V when DNA is added to the solution. The positive peak potential shift of + 60 mV could be associated with the interaction mode, since positive potential shifting is indicative of the intercalation or groove binding mode, ruling out electrostatic interactions [22,42]. This result may be expected due to the electrostatic repulsion between the negatively charged phosphate group from DNA and the sulfonate group from TZ. From this point of view, the problem is reduced to identifying if the interaction mode is through groove binding or intercalation.

Once it was established that TZ interacts with DNA, we evaluated the optimal interaction time of the process to continue with the characterization. In this case, the voltammetric signal of TZ after the interaction with DNA was followed at different interaction times for one hour (Fig. S2a). The initial current value of TZ in the absence of DNA (t = 0) quickly decays after 2 min of interaction with DNA, indicating a fast interaction between both molecules, with a minimum value obtained between 10 and 15 min. At higher interaction times, the reduction signal of TZ slightly increases, but the initial current value is never reached. Therefore, for the following experiments, the optimal experimental interaction time was set to 15 min since the decay in current is the highest with a low RSD value (3 %). Additionally, this time coincides with the time used to purge the solution with nitrogen. Therefore, this interaction time also allows the solution to be completely degassed, avoiding the presence of oxygen to prevent the interference of the oxygen reduction reaction.

To confirm the binding of TZ to DNA, voltammetric changes were obtained after adding increasing amounts of DNA to a fixed concentration of TZ using 15 min of interaction time (Fig. 1d). The DP voltammograms of TZ showed a positive shift in potential and an increase in the peak current value. In some cases, it is possible to observe two overlapping peaks; this could be related to the reduction of TZ molecules that are interacting with DNA and the reduction of free TZ molecules. The peak potential shift suggests an interaction mode via intercalation between base pairs of DNA or via groove binding [22,43].

To identify which of these modes is predominant, the experiment reported in Fig. 1d was repeated but in the presence of 90 mM NaCl to increase the ionic strength of the medium (Fig. S3a). The resulting voltammograms showed an improvement in the peak definition and higher current values than those obtained without NaCl, indicating that the interaction of TZ with DNA depends on the ionic strength. Additionally, a positive potential shift was observed in the presence and absence of NaCl. The addition of strong electrolytes such as NaCl will affect the interaction between DNA and molecules that have a groove binding mode instead of intercalation; the presence of Na^+ partly shields the negative charges of the DNA, reducing the electrostatic effects that affect the external interaction between molecules and DNA [44]. If TZ was intercalated in the DNA, the IS would not have an effect on the electrochemical response of TZ; therefore, the results suggest an interaction mode via groove binding.

Assuming that small molecules produce a single complex with DNA, their interaction can be described as:

$$molecule + DNA \rightleftharpoons molecule - DNA \quad (3)$$

Under the assumption of reversible, diffusion-controlled electron transfer and the complex of TZ-DNA being a 1:1 association complex, the titration of TZ with different concentrations of DNA can be described by the current titration equation [7,45]:

$$log\left(\frac{1}{[DNA]}\right) = logK + log\left(\frac{I}{I_0 - I}\right) \quad (4)$$

where K is the binding constant, I is the maximum current observed in the presence of DNA, I_0 is the current observed in the absence of DNA, and [DNA] is the molar concentration of DNA. From the slope of a plot of

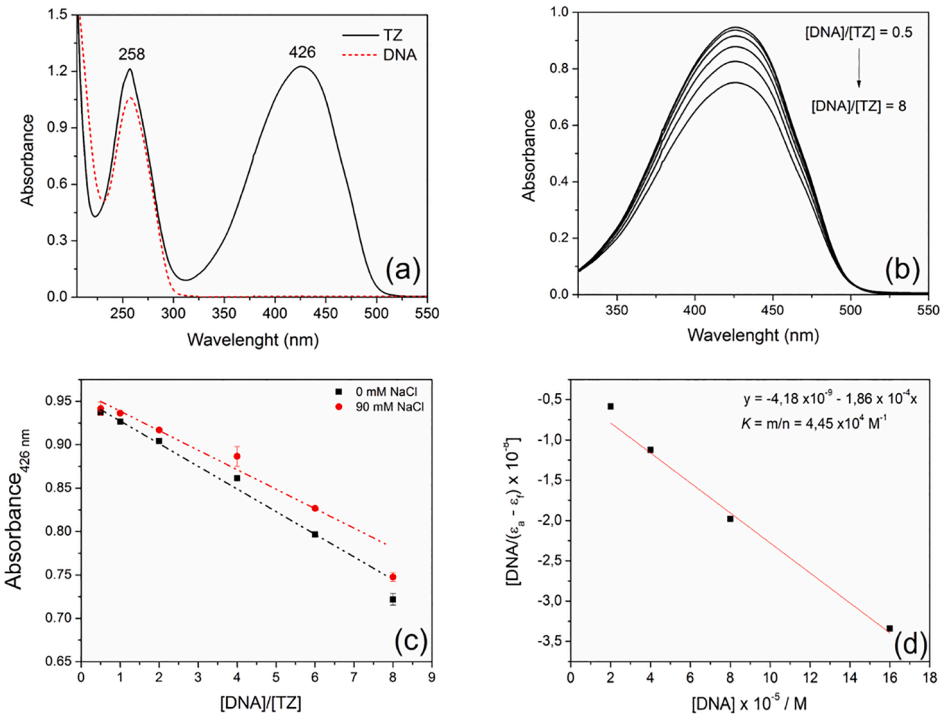


Fig. 2. (a) UV–visible spectra of 0.05 mM TZ and 0.15 mM DNA. (b) Changes in the UV–visible spectra of TZ upon addition of increasing concentration of DNA; r_i = DNA/TZ = 0.5, 1, 2, 3, 4, 6 and 8. Interaction time: 5 min. (c) Effect of ionic strength r_i = DNA/TZ = 0.5, 1, 2, 3, 4, 6 and 8; the measurements were made without NaCl and with 90 mM NaCl. (d) Determination of the association constant of TZ-DNA. All experiments were performed in 0.1 M PBS (pH 7.4).

$1/[DNA]$ versus $log(\frac{I}{I_0-I})$, it is possible to determine the binding constant. According to this, the calculated value of K was $5.75x10^4M^{-1}$, obtained from the correlation plot shown in Fig. S3b.

3.2. Interaction of TZ and DNA by spectroscopic studies

In Fig. 2a, it is observed that TZ exhibited two well-defined absorption peaks at 258 and 426 nm, in contrast with DNA that presented only one at 258 nm. The interaction between TZ and DNA was evaluated following the changes in the TZ absorption band at 426 nm since it provided an easy way to monitor the changes in the absorption spectra upon increasing concentrations of DNA [46]. The experiments were performed after adding increasing amounts of DNA to a fixed concentration of TZ.

First, we evaluated the dilution of TZ upon water addition (not shown), and the results showed a slight decrease in absorbance (<1%), therefore, the hypochromic effect observed due the dilution of TZ is very low. After the interaction of TZ with different DNA concentrations, the absorption band of TZ at 426 nm decreases, producing a hypochromic change of approximately 23 % (Fig. 2b), similar to what has been observed for other azo colorants with DNA [47]. Other authors stated that this result indicates that TZ interacts with DNA by an intimate overlap of the π electrons of the aromatic groups of TZ and the DNA base pair [6,9,17], but this is true only for an intercalation mode. Additionally, for the intercalation mode, new bands and/or batho- or hypsochromic shifts are expected with increasing amounts of DNA [48]. In this case, no new bands or displacements in the maximum absorbance were observed; therefore, an intercalation mode was dismissed, as we will also demonstrate through our computational models. Moreover, the hypochromism effect could be associated with an external interaction, such as groove binding.

Similar to the electrochemical results, to verify that the interaction mode is groove binding, the effect of the IS was studied (Fig. 2c). The presence of NaCl induced an increase in absorbance when compared to the effect of DNA in the absence of NaCl. This result is in agreement with the electrochemical experiments and confirms an interaction mediated by groove binding since TZ interacts externally with the grooves of DNA and consequently is more exposed to ionic force charges. According to these results, the changes in current and absorbance suggest that the increase in the IS induces the dissociation of TZ from the DNA groove binding site, augmenting the availability of TZ in its free form.

The binding constant (K) was determined from the spectral titration data using the Wolfe-Shimer equation [49]:

$$\frac{(DNA)}{(\varepsilon_a-\varepsilon_f)}=\frac{(DNA)}{(\varepsilon_b-\varepsilon_f)}+\frac{1}{K(\varepsilon_b-\varepsilon_f)} \quad (5)$$

where (DNA) is the concentration of DNA, ε_a is the apparent absorption coefficient ($A_{obs}/(M)$), ε_f is the extinction coefficient of the free molecule and ε_b is the extinction coefficient of the molecule when fully bound to DNA. In a plot of $(DNA)/(\varepsilon_a-\varepsilon_f)$ versus (DNA), the constant (K) is given by the ratio of the slope to the intercept [16,17,19,20]. The K value obtained was $4.45x10^4M^{-1}$, close to the value obtained by the electrochemical method.

3.3. Modelling of the DNA-TZ complex

To provide a molecular basis for the binding mode of TZ on DNA, a molecular modeling study was carried out to identify the most likely mode of interaction by identifying the complex capable of reproducing the experimental observations. From the 30 docking conformations, 10 conformations proved to be stable during the 4 ns of MD simulation, from which one was eliminated because two complexes were identical in their binding mode and intermolecular interactions with DNA. From the 9 selected complexes shown in Fig. 3a, one corresponded to the π-π interaction conformation at the higher end of the DNA (**conf1**), five corresponded to minor groove binding (**conf2** to **conf6**), one corresponded to π-π/hydrogen bond interactions in the middle region of the DNA (**conf7**), one corresponded to major groove binding (**conf8**), and one corresponded to intercalation in the middle region (**conf9**). In terms of the groove binding complexes, as the extension of the minor groove

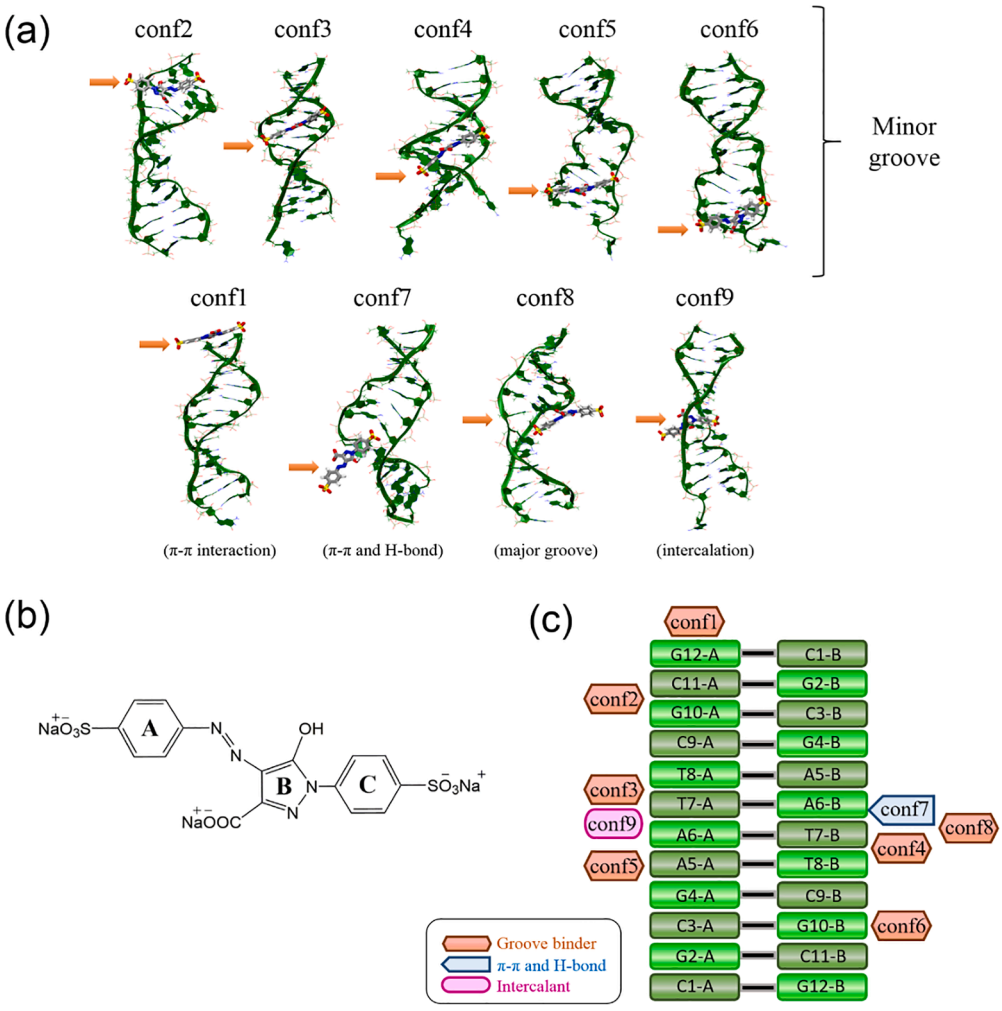


Fig. 3. (a) Optimized geometries of the nine conformations representing the complete series of possible binding modes of TZ with the ds-DNA structure. The orange arrow indicates the location of the TZ molecule. In the upper region, there are minor groove binding modes along the whole extension of the ds-DNA structure, whereas in the lower region, there are four distinct possible binding modes, including the interaction with the end of the ds-DNA structure (**conf1**), major groove binding (**conf8**) and intercalation (**conf9**) (green: DNA structure; TZ: silver-carbon, red-oxygen and blue-nitrogen). (b) Molecular structure of tartrazine (A and C = sulfonatophenyl rings; B = pyrazolone ring). (c) Scheme representing the ds-DNA sequence used in this study, together with the location of TZ for the different binding modes modeled here.

Table 1
Interaction energies of the TZ-DNA complexes. ΔE_{rel} is defined as the interaction energy difference between **conf1** used as the baseline and the corresponding energy of each complex.

Complex	E_{int} (kcal/mol)	ΔE_{rel} (kcal/mol)
Conf1	−75.6	0
Conf2	−181.9	−106.3
Conf3	−269.1	−193.5
Conf4	−281.2	−205.6
Conf5	−199.7	−124.1
Conf6	−196.6	−121.0
Conf7	−104.8	−29.2
Conf8	−248.9	−173.3
Conf9	−190.2	−114.6

binding sites in the 12-mer sequence was larger, it was possible to find several binding modes along the whole extension of the DNA structure. Meanwhile, for the major groove, only one stable conformation was obtained at the unique major groove site present in the structure used here.

To rationalize the preference toward certain binding modes according to their intermolecular interactions, we calculated an estimate of the interaction energies as described in the methodology section and listed in Table 1. According to this, we discussed their relative magnitudes with respect to the specific interaction formed between TZ (Fig. 3b) and the DNA of each complex. This will shed light on the interaction pattern that dominates the complex formation.

Conf1 is characterized by a π-π interaction between the pyrazolone from TZ and the guanine (G) from chain A of the DNA (G12-A, Fig. 3c). However, it is possible for this interaction to transition between the other aromatic rings from TZ and the DNA base pair. As TZ only interacted through one side and no hydrogen bonds were formed, this was the lowest interaction energy obtained, with a value of −75.6 kcal/mol. This will be the reference value defined as zero to facilitate the analysis of the rest of the complexes, where more negative values mean more stability than **conf1** in the magnitude. For **conf2**, a minor groove binding complex, it was possible to find the formation of a hydrogen bond between the pyrazolone –OH group and the deoxyribose from cytosine (C) (C11-A). A second hydrogen bond between the carboxylate from pyrazolone and the amino-purine moiety from G4-B was found, and a third hydrogen bond was formed between the azo moiety and the amino-purine from G10-A. The rest are dispersion interactions driven by the sulfonatophenyl rings and the deoxyribose from G10-A and C3-B from the DNA backbone. These interactions led to an increase of −106.3 kcal/mol compared to that of **conf1**. Within the complexes interacting through a minor groove, **conf3** seems to be deeply buried into the cleft, with both ends from the TZ molecule denoted by the sulfonate groups anchored through hydrogen bonds with the –OH group from the deoxyribose of thymine (T) from chain A (T7-A) at one end and the other by interacting with the amino-purine from G4-B. A hydrogen bond between the –OH group from pyrazolone and the carbonyl group from the methyl-pyrimidine ring of T8-A is formed; therefore, **conf3** has a total of 3 hydrogen bonds as part of the interaction network. As expected, it showed a large increase of −193.5 kcal/mol in the interaction

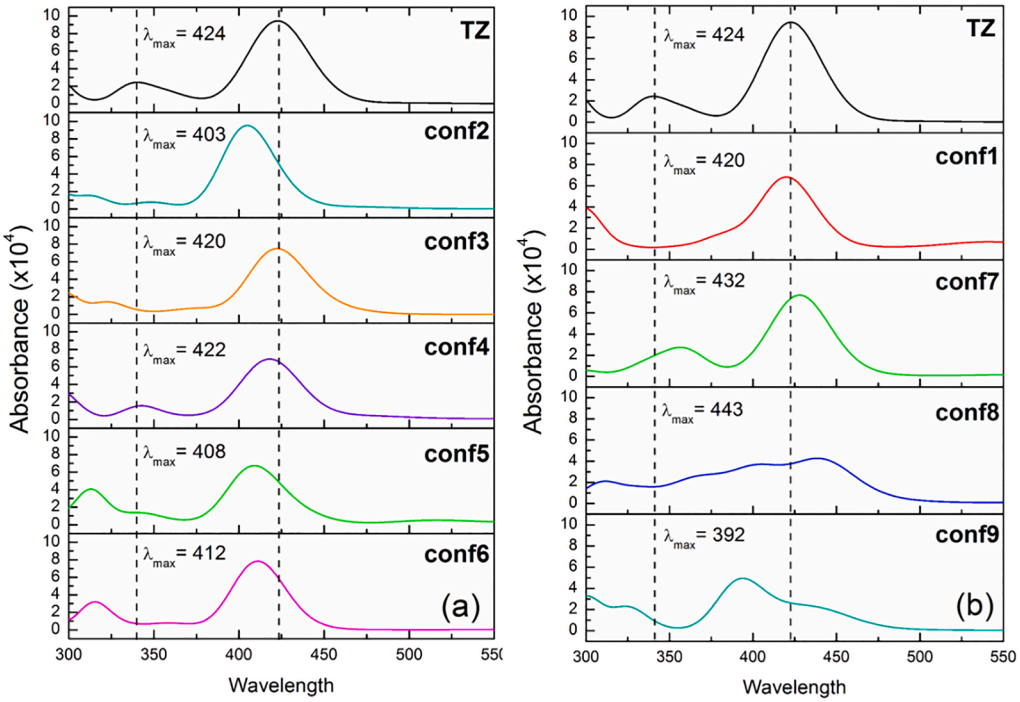


Fig. 4. Simulated UV–visible spectra of TZ and TZ-DNA complexes with the different interaction modes studied here. (a) Models representing the minor groove binding modes. (b) Models representing distinct binding modes, such as interaction with the end of the ds-DNA structure (**conf1**), major groove binding (**conf8**) and intercalation (**conf9**).

energy compared to that of **conf1**. The next complex in the minor groove series is **conf4**, which forms a hydrogen bond between one sulfonate group and the –OH from the deoxyribose from T8-B and a hydrogen bond between one nitrogen group of the azo moiety and the –OH from the deoxyribose from T7-A. The sulfonatophenyl rings seem to be interacting through dispersion forces with the DNA backbone. The interaction energy increase from **conf1** was very close to that obtained for **conf3**, with a value of −205.6 kcal/mol. Regarding **conf5**, its interaction is mainly dominated by dispersive interactions with no hydrogen bonds involved, where the TZ interacts through one of its sides toward the minor groove, probably because in this conformation, it is best fitted into the binding site. This is reflected by the decrease in the relative interaction energy with respect to those of **conf3** and **conf4**, with a value of −124.1 kcal/mol over that of **conf1**. Similar to **conf5, conf6** seems to be mainly dominated by dispersion forces between TZ and the DNA backbone, where the only hydrogen bond is formed between the –OH group from pyrazolone and the hydroxyl from deoxyribose from G10-B. Consequently, **conf5** and **conf6** showed close magnitudes in their interaction energies. The **conf7** complex is characterized by the TZ only half interacting with the DNA, leaving the second sulfonatophenyl ring toward the solvent. This may represent an intermediate conformation state before full incorporation into the minor groove. The sulfonate group inside the minor groove interacts with the –OH group from deoxyribose from T7-B. A π-π interaction between the sulfonatophenyl ring and the adenine ring from A5-A is formed, together with a hydrogen bond between the pyrazolone carboxylate group and the –OH group from the deoxyribose from A5-A. Interestingly, this complex showed only slightly higher interaction energies than that of **conf1,** with an increase of only −29.2 kcal/mol. These results suggest that the binding process may be initiated by the formation of a π-π interaction between the sulfonatophenyl ring and the ring from the nucleotide base, which is later replaced by the formation of a more intricate hydrogen bond network, as evidenced for **conf3**. The model representing the major groove binding, namely, **conf8,** is characterized by the formation of several hydrogen bonds, among which there is an interaction between the sulfonate with both the pyrimidine ring from T7-B and the aminopurine ring from A6-B. Additionally, a hydrogen bond exists between the pyrazolone –OH group and the phosphate from A5-B. The rest of the interactions are of a dispersive nature mainly with the backbone of chain B. The magnitude of the interaction energy is only slightly lower than that obtained for **conf3** and **conf4**, revealing that this complex would be able to contribute to the experimental observations. Finally, **conf9** corresponds to an intercalation binding mode. Due to the reduced size of the DNA structure, the only stable intercalation complex was obtained in the middle region of the sequence, as it was able to provide enough space without excessively distorting the DNA structure. This interaction mode is characterized by the π- stacking conformation of one sulfonatophenyl ring between the pyrimidine rings of T7-A and T7-B. No hydrogen bonds were formed in this binding mode, which showed a lower interaction energy when compared to those of **conf3** and **conf4**, ruling out its contribution to the experimental results. In general, the binding of TZ to the DNA structure is dominated by the formation of hydrogen bonds between the sulfonate groups from TZ and the deoxyriboses from DNA, and an important involvement of the pyrazolone ring in this hydrogen bonding network was also found. Most of the interaction takes place with the –OH groups from the deoxyriboses, and a minor involvement from the base pair was found. A preference toward zones rich in adenine and thymine was observed, as pinpointed in Fig. 3c. Finally, according to the interaction strengths, there is a clear preference toward interacting with the middle region of the DNA structure, involving both the minor groove binding mode (**conf3** and **conf4**) and the major groove binding mode (**conf8**).

3.4. UV–visible spectra calculation of the DNA-TZ complexes

To define the most likely binding modes of TZ to the DNA sequence used here, we calculated the UV–vis spectrum of each complex to determine which binding conformation better represents and contributes to the experimental optical response. According to the experimental data, the main absorption band associated with the TZ molecule and used to follow its behavior during TZ binding to DNA appeared at 426 nm. As listed in Table S1, for the TZ molecule in implicit water solvent,

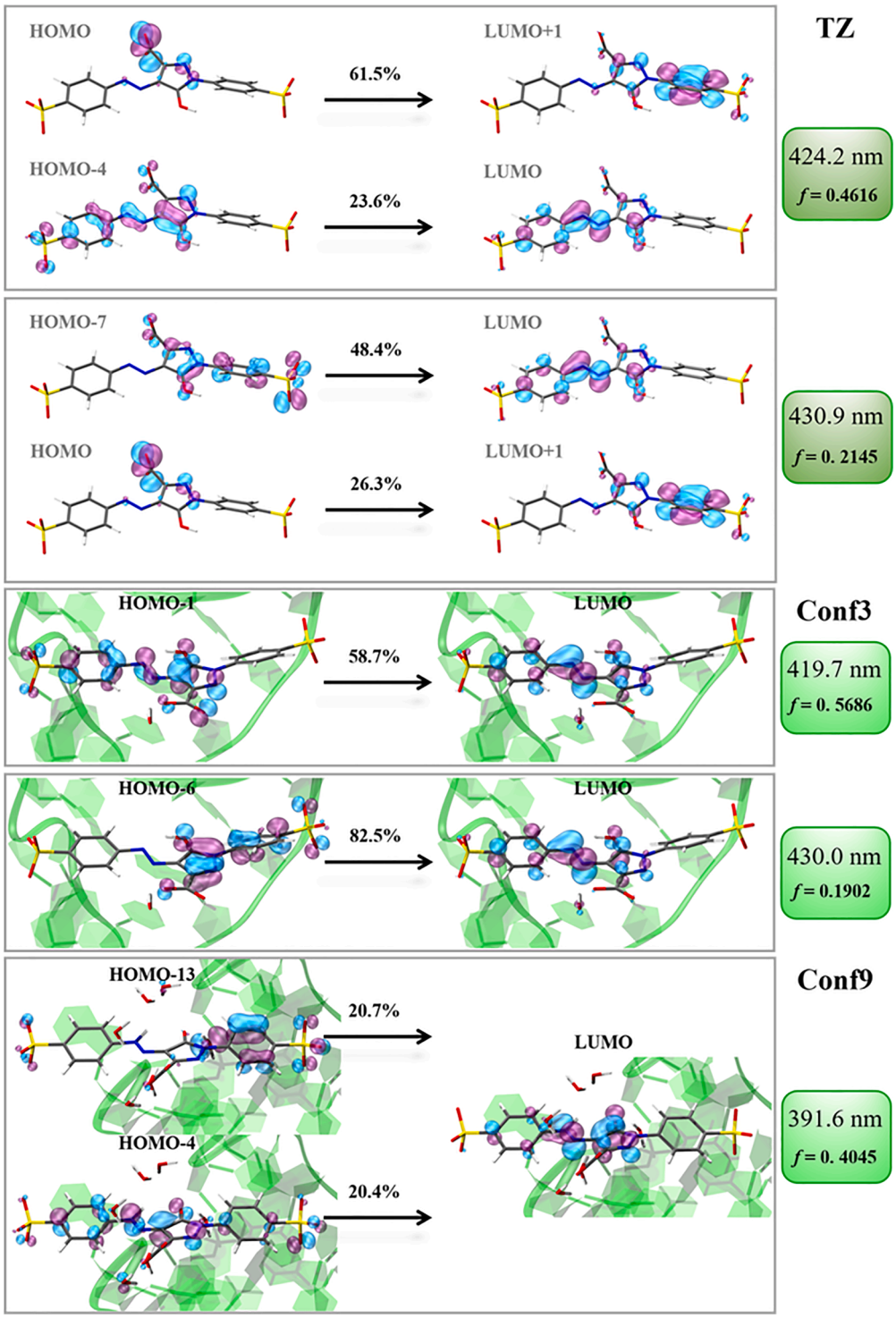


Fig. 5. Molecular orbital representation for the electronic transitions of TZ and TZ-DNA complexes (**conf3** and **conf9**) necessary to characterize the main absorption band experimentally observed from UV–vis experiments used to rationalize the TZ-DNA binding mode.

the main absorption band was located at 424 nm. This result is in close agreement with the experimental data, reinforcing the suitability of the methodology and providing the baseline for the analysis of the changes in the calculated optical response after binding to the DNA. The simulated spectra are depicted in Fig. 4 and are contrasted with the spectrum of TZ in implicit solvent.

For the complexes representing a minor groove binding mode (**conf2** to **conf6**, Fig. 4a), only **conf2** showed a blueshift close to 20 nm, without the experimentally observed hypochromic effect. The blueshift may be related to the direct interaction of the azo moiety with G10-A, which can change the energy of the molecular orbitals involving this moiety. The rest of the TZ complexes interacting through the minor groove binding mode (**conf3** to **conf6**) are close to the experimental behavior in terms of the hypochromic effect. Among these, **conf3** is the best model reproducing the exact behavior observed from the experiment, where only a reduction of the main band at 426 nm is observed. This model corresponds to a minor groove binding mode in the middle region of the DNA structure, in line with the experimental findings exposed above

regarding the preferred binding mode. Interestingly, **conf1**, which is characterized by π-interactions at the upper end of the ds-DNA structure, also showed a similar absorption band compared to some minor groove binding modes. According to this, it would be expected that the experimental observable is a consequence of a contribution to a minor extent from **conf1** and **conf4** and a major contribution from **conf3**. On the other hand, **conf5** and **conf6**, which are in the lower region, suffer from a blueshift ranging between 12 and 16 nm, which does not contribute to the experimental spectrum. Meanwhile, **conf7**, which represents a possible transition but a stable conformation prior to adopting a full minor groove binding mode, showed a similar behavior to **conf3** with a slight redshift in the main absorption band, as shown in Fig. 4b. According to the theoretical results, the major groove binding mode represented by **conf8** showed a large decrease in the main absorption band with a redshift to 443.4 nm accompanied by the emergence of a second and shorter band at a higher energy located at 403.8 nm. This indicates that this binding mode is less likely to contribute to the experimental behavior when compared to the minor groove binding mode. One of the main questions to be addressed here was to define the dominant binding mode of TZ with DNA, and for this, we have **conf9**, with which we were capable of modeling the expected spectrum in the case of an intercalation binding mode. As a result, it was found that the main absorption band was redshifted to 391.7 nm, with the appearance of a second shorter band at 448.0 nm at lower energy. Our results suggest that the lack of experimental evidence showing a contribution from this optical response behavior points toward the lack of an intercalation mode of binding by TZ.

From the analysis of the nature of the electronic transitions involved in the main UV–vis band followed for the binding process, it is possible to provide insights into the chemical role of the intermolecular interactions between TZ and DNA and the changes in the optical response. The molecular orbital representations for the TZ molecule, **conf3** and **conf9** are depicted in Fig. 5, and those for the rest of the complexes are in the Supporting Information (Figure S4).

The main electronic transition from the TZ molecule showed a $\pi \rightarrow \pi^*$ character in one case involving the pyrazolone ring with the sulfonatophenyl ring (C) and in another case involving the azo moiety. In this sense, the main orbital feature observed among the minor groove complexes that were close to the experimental response (**conf3** and **conf4**) is that all have an electronic transition from π-sulfonatophenyl ring (A) + π-azo + π-pyrazolone to π*-sulfonatophenyl ring (A) + π*-azo + π*-pyrazolone. For **conf1**, in which its spectrum was also similar to the experimental spectrum, the arrival orbital also involved a π*-azo contribution, although the rest of the contributions were of π-bonding character.

The electronic transition between the free TZ and the molecule in the complex with DNA seems to be similar in nature, where the main common feature is the involvement of the azo moiety, which does not strongly interact with the DNA base pairs. Despite the mixed nature of some of the electronic transitions of several complexes, a common pattern is always associated with the π-azo to π*-azo character of the main band observed in the UV–vis spectrum. For the intercalation binding mode, the involvement of the π-character transition with a lack of azo moiety contribution denotes the effect that the π-stacking interactions would have on these types of compounds, with the consequent increase in the energy difference between the occupied molecular orbitals with π-bonding character and the LUMO/LUMO + 1 molecular orbital, probably because of the stabilization and decrease in energy of the HOMO and its closer occupied orbitals. Finally, the low interaction strength between TZ and DNA for **conf1** explains the lack of change in the electronic transition mechanism, which was indeed observed for the fully intercalated complex represented by **conf9**.

4. Conclusion

A detailed electrochemical, UV–vis spectroscopy and computational multiscale modeling exploration of TZ and ds-DNA binding was presented, and the results revealed an interaction mechanism through a minor groove binding mode. DPV experiments showed that after the addition of DNA, the TZ peak current showed a positive shift in potential and an increase in the peak current value. On the other hand, UV–vis spectroscopy spectra of the TZ-DNA interaction showed a hypochromic effect without a shift in the bands or the appearance of any new band. The ionic strength studies showed that the increase in the concentration of NaCl increased both the current and the absorption band in both the electrochemical and UV–vis experiments, suggesting the dissociation of the TZ-DNA complex and pointing out that TZ interacts with the surface of the double-stranded DNA structure without intercalation. This was also supported by the lack of displacement of the absorption band expected for the intercalation mode due to the π-stacking interactions, also evidenced from the computational models. The QM/MM calculations allowed us to specify the preference toward minor groove binding sites in the double-stranded DNA structure by exposing that these models were the only ones capable of accurately reproducing the experimental UV–vis spectrum. In addition, we found that TZ presented some degree of sequence selectivity, where TZ showed some preference toward the region rich in adenine and thymine. Our results provide the grounds to define that the minor groove binding mode of TZ with DNA correlates with a hypochromic effect, thus solving the discrepancy between the binding of TZ to double stranded DNA and the expected optical response due to complex formation. Finally, the binding constant between TZ and DNA was experimentally calculated as $5.75x10^4M^{-1}$ (DPV) and $4.45x10^4M^{-1}$ (UV–vis), showing the usefulness of the electrochemical method that offers a fast and simple response in this type of study.

CRediT authorship contribution statement

S. Arsenault-Escobar: Validation, Formal analysis, Data curation, Visualization. **J.F. Fuentes-Galvez:** Validation, Formal analysis, Data curation, Visualization. **C. Orellana:** Software, Validation, Formal analysis, Data curation, Visualization. **S. Bollo:** Methodology, Resources, Writing – original draft. **P. Sierra–Rosales:** Conceptualization, Methodology, Validation, Formal analysis, Investigation, Resources, Data curation, Writing – original draft, Writing – review & editing, Visualization, Supervision, Project administration, Funding acquisition. **S. Miranda-Rojas:** Conceptualization, Methodology, Software, Validation, Formal analysis, Investigation, Resources, Data curation, Writing – original draft, Writing – review & editing, Visualization, Supervision, Project administration, Funding acquisition.

Declaration of Competing Interest

The authors declare that they have no known competing financial interests or personal relationships that could have appeared to influence the work reported in this paper.

Acknowledgements

This work was funded by FONDECYT-Chile (Grant No. 11170901 and No. 1200828). This research was supported by the high-performance computing system of PIDi-UTEM (SCC-PIDi-UTEM - CONICYT - FONDEQUIP - EQM180180) and CONICYT-FONDEQUIP EQM140112. Powered@NLHPC: This research was partially supported by the supercomputing infrastructure of the NLHPC (ECM-02).

Appendix A. Supplementary material

Supplementary data to this article can be found online at https://doi.org/10.1016/j.saa.2023.122400.

References

[1] A. Basu, G. Suresh Kumar, Multispectroscopic and calorimetric studies on the binding of the food colorant tartrazine with human hemoglobin, J. Hazard. Mater. 318 (2016) 468–476, https://doi.org/10.1016/j.jhazmat.2016.07.023.

[2] H.T. El-borm, G.M. Badawy, S.H. El-nabi, W.A. El-sherif, M.N. Atallah, Toxicity of Sunset Yellow FCF and Tartrazine dyes on DNA and cell cycle of liver and kidneys of the chick embryo: The alleviative effects of Curcumin, Egypt J. Zool. 74 (2020) 43–55, https://doi.org/10.12816/ejz.2020.42218.1040.

[3] T.E. Journal, Opinion of the Scientific Panel on food additives, flavourings, processing aids and materials in contact with food (AFC) to review the toxicology of a number of dyes illegally present in food in the EU, EFSA J. 3 (2005) 263, https://doi.org/10.2903/j.efsa.2005.263.

[4] X. Pan, P. Qin, R. Liu, J. Wang, Characterizing the interaction between tartrazine and two serum albumins by a hybrid spectroscopic approach, J. Agric. Food Chem. 59 (2011) 6650–6656, https://doi.org/10.1021/jf200907x.

[5] A. Basu, G. Suresh Kumar, Binding and Inhibitory Effect of the Dyes Amaranth and Tartrazine on Amyloid Fibrillation in Lysozyme, J. Phys. Chem. B. 121 (2017) 1222–1239, https://doi.org/10.1021/acs.jpcb.6b10465.

[6] A. Basu, G.S. Kumar, Studies on the interaction of the food colorant tartrazine with double stranded deoxyribonucleic acid, J. Biomol. Struct. Dyn. 34 (2016) 935–942, https://doi.org/10.1080/07391102.2015.1057766.

[7] S. Asaadi, R. Hajian, DNA binding studies of Sunset Yellow FCF using spectroscopy, viscometry and electrochemical techniques, J. Mol. Struct. 1146 (2017) 861–867, https://doi.org/10.1016/j.molstruc.2017.06.065.

[8] Y. Ma, G. Zhang, J. Pan, Spectroscopic studies of DNA interactions with food colorant indigo carmine with the use of ethidium bromide as a fluorescence probe, J. Agric. Food Chem. 60 (2012) 10867–10875, https://doi.org/10.1021/jf303698k.

[9] P. Mpountoukas, A. Pantazaki, E. Kostareli, P. Christodoulou, D. Kareli, S. Poliliou, C. Mourelatos, V. Lambropoulou, T. Lialiaris, Cytogenetic evaluation and DNA interaction studies of the food colorants amaranth, erythrosine and tartrazine, Food Chem. Toxicol. 48 (2010) 2934–2944, https://doi.org/10.1016/j.fct.2010.07.030.

[10] K. De la Cruz Morales, G. Alarcón-Angeles, A. Merkoçi, Nanomaterial-based Sensors for the Study of DNA Interaction with Drugs, Electroanalysis 31 (2019) 1845–1867, https://doi.org/10.1002/elan.201900286.

[11] S. Campuzano, M. Pedrero, J.M. Pingarrón, Electrochemical nucleic acid-based biosensing of drugs of abuse and pharmaceuticals, Curr. Med. Chem. 25 (2018) 4102–4118, https://doi.org/10.2174/0929867324666171121103156.

[12] M. Sirajuddin, S. Ali, A. Badshah, Drug-DNA interactions and their study by UV-Visible, fluorescence spectroscopies and cyclic voltametry, J. Photochem. Photobiol. B Biol. 124 (2013) 1–19, https://doi.org/10.1016/j.jphotobiol.2013.03.013.

[13] A. Rescifina, C. Zagni, M.G. Varrica, V. Pistarà, A. Corsaro, Recent advances in small organic molecules as DNA intercalating agents: Synthesis, activity, and modeling, Eur. J. Med. Chem. 74 (2014) 95–115, https://doi.org/10.1016/j.ejmech.2013.11.029.

[14] S.U. Rehman, T. Sarwar, M.A. Husain, H.M. Ishqi, M. Tabish, Studying non-covalent drug-DNA interactions, Arch. Biochem. Biophys. 576 (2015) 49–60, https://doi.org/10.1016/j.abb.2015.03.024.

[15] E. Horakova, V. Vyskocil, J. Barek, Interaction study of methyl violet 2B with DNA and voltammetric determination of DNA in aqueous solutions, Monatsh. Chem. 147 (2016) 119–126, https://doi.org/10.1007/s00706-015-1590-9.

[16] S. Kashanian, S. Heidary Zeidali, K. Omidfar, N. Shahabadi, Multi-spectroscopic DNA interaction studies of sunset yellow food additive, Mol. Biol. Rep. 39 (12) (2012) 10045–10051.

[17] S. Kashanian, S.H. Zeidali, DNA Binding Studies of Tartrazine Food Additive, DNA Cell Biol. 30 (2011) 499–505, https://doi.org/10.1089/dna.2010.1181.

[18] A. Basu, G. Suresh Kumar, Minor groove binding of the food colorant carmoisine to DNA: Spectroscopic and calorimetric characterization studies, J. Agric. Food Chem. 62 (2014) 317–326, https://doi.org/10.1021/jf404960n.

[19] M. Arvin, G. Dehghan, M.A. Hosseinpourfeizi, A.A. Moosavi-Movahedi, Spectroscopic and Electrochemical Studies on the Interaction of Carmoisine Food Additive with Native Calf Thymus DNA, Spectrosc. Lett. 46 (2013) 250–256, https://doi.org/10.1080/00387010.2012.723663.

[20] S. Alamatsaz, N. Rasouli, N. Sohrabi, Binding thermodynamic and spectroscopic of Allura Red AC to Calf thymus DNA, Pharm. Chem. J. 3 (2016) 48–57.

[21] P. Sierra-Rosales, C. Berríos, S. Miranda-Rojas, J.A. Squella, Experimental and theoretical insights into the electrooxidation pathway of azo-colorants on glassy carbon electrode, Electrochim. Acta. 290 (2018) 556–567, https://doi.org/10.1016/j.electacta.2018.09.090.

[22] M. Catalán, A. Álvarez-lueje, S. Bollo, Electrochemistry of interaction of 2- (2-nitrophenyl) -benzimidazole derivatives with DNA, Bioelectrochemistry 79 (2010) 162–167, https://doi.org/10.1016/j.bioelechem.2010.02.002.

[23] L. Fang, W. Wang, P. He, L. Du, Y. Yuan, Interaction of nimodipine with DNA investigated by electrochemical methods, ECS Trans. 35 (2011) 3–12, https://doi.org/10.1149/1.3653209.

[24] K. Morawska, T. Popławski, W. Ciesielski, S. Smarzewska, Interactions of lamotrigine with single- and double-stranded DNA under physiological conditions, Bioelectrochemistry 136 (2020), 107630, https://doi.org/10.1016/j.bioelechem.2020.107630.

[25] P.O. Vardevanyan, A.P. Antonyan, M.A. Parsadanyan, K.V. Pirumyan, A. M. Muradyan, A.T. Karapetian, Influence of ionic strength on hoechst 33258 binding with dna, J. Biomol. Struct. Dyn. 25 (2008) 641–646, https://doi.org/10.1080/07391102.2008.10507210.

[26] H.R. Drew, R.M. Wing, T. Takano, C. Broka, S. Tanaka, K. Itakura, R.E. Dickerson, Structure of a B-DNA dodecamer: conformation and dynamics, Proc. Natl. Acad. Sci. 78 (4) (1981) 2179–2183.

[27] W. Humphrey, A. Dalke, K. Schulten, VMD: Visual molecular dynamics, J. Mol. Graph. 14 (1996) 33–38, https://doi.org/10.1016/0263-7855(96)00018-5.

[28] J.C. Phillips, R. Braun, W. Wang, J. Gumbart, E. Tajkhorshid, E. Villa, C. Chipot, R. D. Skeel, L. Kalé, K. Schulten, Scalable molecular dynamics with NAMD, J. Comput. Chem. 26 (16) (2005) 1781–1802.

[29] K. Hart, N. Foloppe, C.M. Baker, E.J. Denning, L. Nilsson, A.D. Mackerell Jr, Optimization of the CHARMM additive force field for DNA: Improved treatment of the BI/BII conformational equilibrium, J. Chem. Theory Comput. 8 (2012) 348–362, https://doi.org/10.1021/ct200723y.

[30] G.M. Morris, R. Huey, W. Lindstrom, M.F. Sanner, R.K. Belew, D.S. Goodsell, A. J. Olson, AutoDock4 and AutoDockTools4: Automated docking with selective receptor flexibility, J. Comput. Chem. 30 (2009) 2785–2791, https://doi.org/10.1002/jcc.21256.

[31] A.D. Becke, Density-functional exchange-energy approximation with correct asymptotic behavior, Phys. Rev. A. 38 (1988) 3098–3100, https://doi.org/10.1103/PhysRevA.38.3098.

[32] J. Perdew, Density-functional approximation for the correlation energy of the inhomogeneous electron gas, Phys. Rev. B. 33 (1986) 8822–8824, https://doi.org/10.1103/PhysRevB.33.8822.

[33] A. Schäfer, H. Horn, R. Ahlrichs, Fully optimized contracted Gaussian basis sets for atoms Li to Kr, J. Chem. Phys. 97 (4) (1992) 2571–2577.

[34] S. Grimme, J. Antony, S. Ehrlich, H. Krieg, A consistent and accurate ab initio parametrization of density functional dispersion correction (DFT-D) for the 94 elements H-Pu, J. Chem. Phys. 132 (15) (2010) 154104.

[35] S. Metz, J. Kästner, A.A. Sokol, T.W. Keal, P. Sherwood, ChemShell—a modular software package for QM/MM simulations, Wiley Interdiscip. Rev. Comput. Mol. Sci. 4 (2014) 101–110, https://doi.org/10.1002/wcms.1163.

[36] F. Furche, R. Ahlrichs, C. Hättig, W. Klopper, M. Sierka, F. Weigend, Turbomole, Wiley Interdiscip. Rev. Comput. Mol. Sci. 4 (2014) 91–100, https://doi.org/10.1002/wcms.1162.

[37] C. Bannwarth, S. Ehlert, S. Grimme, GFN2-xTB—An Accurate and Broadly Parametrized Self-Consistent Tight-Binding Quantum Chemical Method with Multipole Electrostatics and Density-Dependent Dispersion Contributions, J. Chem. Theory Comput. 15 (2019) 1652–1671, https://doi.org/10.1021/acs.jctc.8b01176.

[38] R. Bauernschmitt, R. Ahlrichs, Treatment of electronic excitations within the adiabatic approximation of time dependent density functional theory, Chem. Phys. Lett. 256 (1996) 454–464, https://doi.org/10.1016/0009-2614(96)00440-X.

[39] M.E. Casida, C. Jamorski, K.C. Casida, D.R. Salahub, Molecular excitation energies to high-lying bound states from time-dependent density-functional response theory: Characterization and correction of the time-dependent local density approximation ionization threshold, J. Chem. Phys. 108 (1998) 4439–4449, https://doi.org/10.1063/1.475855.

[40] T. Bruhn, A. Schaumlöffel, Y. Hemberger, G. Bringmann, SpecDis: Quantifying the Comparison of Calculated and Experimental Electronic Circular Dichroism Spectra, Chirality 25 (2013) 243–249, https://doi.org/10.1002/chir.22138.

[41] J.J. Gooding, R.G. Compton, C.M. Brennan, J.H. Atherton, The mechanism of the electro-reduction of some azo dyes, Electroanalysis 8 (1996) 4–8, https://doi.org/10.1002/elan.1140080604.

[42] A. Shah, E. Nosheen, S. Munir, A. Badshah, R. Qureshi, Z.-u. Rehman, N. Muhammad, H. Hussain, Journal of Photochemistry and Photobiology B : Biology Characterization and DNA binding studies of unexplored imidazolidines by electronic absorption spectroscopy and cyclic voltammetry, J. Photochem. Photobiol. B Biol. 120 (2013) 90–97.

[43] S. Kashanian, J.E.N. Dolatabadi, DNA binding studies of 2-tert-butylhydroquinone (TBHQ) food additive, Food Chem. 116 (2009) 743–747, https://doi.org/10.1016/j.foodchem.2009.03.027.

[44] L.A. Reis, M.S. Rocha, DNA interaction with DAPI fluorescent dye: Force spectroscopy decouples two different binding modes, Biopolymers 107 (2017) 1–8, https://doi.org/10.1002/bip.23015.

[45] M.S. Ibrahim, Voltammetric studies of the interaction of nogalamycin antitumor drug with DNA, Anal. Chim. Acta. 443 (2001) 63–72, https://doi.org/10.1016/S0003-2670(01)01184-9.

[46] F. Macii, T. Biver, Spectrofluorimetric analysis of the binding of a target molecule to serum albumin : tricky aspects and tips, J. Inorg. Biochem. 216 (2021), 111305, https://doi.org/10.1016/j.jinorgbio.2020.111305.

[47] A. Basu, G.S. Kumar, Study on the interaction of the toxic food additive carmoisine with serum albumins: A microcalorimetric investigation, J. Hazard. Mater. 273 (2014) 200–206, https://doi.org/10.1016/j.jhazmat.2014.03.049.

[48] Y. Jiang, Y. Yuan, K. Wang, H. Li, C. Xu, X. Yang, Spectroscopic and electrochemical studies on the binding of pyrocatechol violet with telomere DNA and its application, Int. J. Electrochem. Sci. 7 (2012) 10933–10951.

[49] A. Wolfe, G.H. Shimer, T. Meehan, Polycyclic aromatic hydrocarbons physically intercalate into duplex regions of denatured DNA, Biochemistry 26 (20) (1987) 6392–6396.